Photoproduction of charmonia and total charmonium-proton cross sections

J. Hüfner,[1,2] Yu. P. Ivanov,[1,2,3] B. Z. Kopeliovich,[2,3] and A. V. Tarasov[1,2,3]
[1]*Institut für Theoretische Physik der Universität, Philosophenweg 19, 69120 Heidelberg, Germany*
[2]*Max-Planck Institut für Kernphysik, Postfach 103980, 69029 Heidelberg, Germany*
[3]*Joint Institute for Nuclear Research, Dubna, 141980 Moscow Region, Russia*
(Received 20 July 2000; published 9 October 2000)

Elastic virtual photoproduction cross sections $\gamma^* p \to J/\psi(\psi')p$ and total charmonium-nucleon cross sections for J/ψ, ψ', and χ states are calculated in a parameter-free way with the light-cone dipole formalism and the same input: factorization in impact parameters, light-cone wave functions for the γ^* and the charmonia, and the universal phenomenological dipole cross section which is fitted to other data. The charmonium wave functions are calculated with four known realistic potentials, and two models for the dipole cross section are tested. Very good agreement with data for the cross section of charmonium photoproduction is found in a wide range of s and Q^2. The inclusion of the Melosh spin rotation increases the ψ' photoproduction rate by a factor of 2–3 and removes previously observed discrepancies in the ψ' to J/ψ ratio in photoproduction. We also calculate the charmonium-proton cross sections whose absolute values and energy dependences are found to correlate strongly with the sizes of the states.

PACS number(s): 13.85.Lg, 13.60.Le

I. INTRODUCTION

The dynamics of production and interaction of charmonia has drawn attention since their discovery back in 1973. As these heavy mesons have a small size it has been expected that hadronic cross sections may be calculated relying on perturbative QCD. The study of charmonium production became even more intense after charmonium suppression had been suggested as a probe for the creation and interaction of the quark-gluon plasma in relativistic heavy-ion collisions [1].

Since we will never have direct experimental information on charmonium-nucleon total cross sections, one has to extract it from other data, for example, from elastic photoproduction of charmonia $\gamma p \to J/\psi(\psi')p$. The widespread belief that one can rely on the vector dominance model (VDM) is based on previous experience with the photoproduction of ρ mesons. However, even a dispersion approach shows that this is quite risky, because the J/ψ pole in the complex Q^2 plane is nearly 20 times farther away from the physical region than the ρ pole. The multichannel analysis performed in [2] demonstrates that the corrections are huge; $\sigma_{tot}^{J/\psi p}$ turns out to be more that 3 times larger than the VDM prediction. Unfortunately, more exact predictions of the multichannel approach, especially for ψ', requires knowledge of many diagonal and off-diagonal amplitudes which are easily summed only if one uses the oversimplified oscillator wave functions and a $q\bar{q}$-proton cross section of the form $\sigma_{q\bar{q}}(r_T) \propto r_T^2$, where r_T is the transverse $q\bar{q}$ separation.

Instead, one may switch to the quark basis, which should be equivalent to the hadronic basis because of completeness. In this representation the procedure of extracting $\sigma_{tot}^{J/\psi p}$ from photoproduction data cannot be realized directly, but has to be replaced by a different strategy. Namely, as soon as one has expressions for the wave functions of charmonia and the universal dipole cross section $\sigma_{q\bar{q}}(r_T,s)$, one can predict both the experimentally known charmonium photoproduction cross sections and the unknown $\sigma_{tot}^{J/\psi(\psi')p}$. If the photoproduction data are well described, one may have some confidence in the predictions for the $\sigma_{tot}^{J/\psi(\psi')p}$. Of course this procedure will be model dependent, but we believe that this is the best use of photoproduction data one can presently make. This program was performed for the first time in [3]. The aim of this paper is not to propose a conceptually new scheme, but to calculate within a given approach as accurately as possible and without any free parameters. Wherever there is room for arbitrariness, such as forms for the color dipole cross section and those for for charmonium wave functions, we use and compare other author's proposals, which have been tested on data different from those used here.

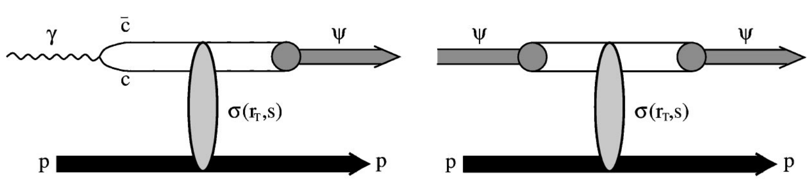

FIG. 1. Schematic representation of the amplitudes for the reactions $\gamma^* p \to \psi p$ (left) and ψp elastic scattering (right) in the rest frame of the proton. The $c\bar{c}$ fluctuation of the photon and the ψ with transverse separation r_T and c.m. energy $\sqrt{s}$ interact with the target proton via the cross section $\sigma(r_T,s)$ and produce a J/ψ or ψ'.

0556-2821/2000/62(9)/094022(12)/$15.00

In the light-cone dipole approach the two processes, photoproduction and charmonium-nucleon elastic scattering look as shown in Fig. 1 [3].

The corresponding expressions for the forward amplitudes read

$$\mathcal{M}_{\gamma^* p}(s,Q^2)=\sum_{\mu,\bar{\mu}}\int_0^1 d\alpha\int d^2\vec{r}_T\Phi_{\psi}^{*(\mu,\bar{\mu})}(\alpha,\vec{r}_T)\times\sigma_{q\bar{q}}(r_T,s)\Phi_{\gamma^*}^{(\mu,\bar{\mu})}(\alpha,\vec{r}_T,Q^2), \tag{1}$$

$$\mathcal{M}_{\psi p}(s)=\sum_{\mu,\bar{\mu}}\int_0^1 d\alpha\int d^2\vec{r}_T\Phi_{\psi}^{*(\mu,\bar{\mu})}(\alpha,\vec{r}_T)\times\sigma_{q\bar{q}}(r_T,s)\Phi_{\psi}^{(\mu,\bar{\mu})}(\alpha,\vec{r}_T). \tag{2}$$

Here the summation runs over spin indexes μ, $\bar{\mu}$ of the c and $\bar{c}$ quarks, Q^2 is the photon virtuality, and $\Phi_{\gamma^*}(\alpha,r_T,Q^2)$ is the light-cone distribution function of the photon for a $c\bar{c}$ fluctuation of separation r_T and relative fraction α of the photon light-cone momentum carried by c or $\bar{c}$. Correspondingly, $\Phi_{\psi}(\alpha,\vec{r}_T)$ is the light-cone wave function of J/ψ, ψ', and χ [only in Eq. (2)]. The dipole cross section $\sigma_{q\bar{q}}(r_T,s)$ mediates the transition (cf. Fig. 1).

In Sec. II we review the status of the factorized light-cone approach to photoproduction of heavy quarkonia. Besides the well-known distribution function of quarks in the photon, it needs knowledge of the universal flavor-independent dipole cross section which depends on the transverse $\bar{q}q$ separation and energy. In Sec. II A we introduce two parametrizations available in the literature.

Making use of the nonrelativistic approximation for heavy quarkonia in Sec. II B we solve the Schrödinger equation with four types of relativistic potentials available in the literature. The next most difficult step is a Lorentz boost to the infinite-momentum frame discussed in Sec. II C. Although this procedure is ill defined and no unambiguous recipe is known, we apply the standard and widely used one. We put a special emphasis on importance of the Melosh spin transformation, which turns out to be very important.

The final expression for the photoproduction cross sections is presented in Sec. III A and results are compared with available data for J/ψ production in Sec. III B. Although the calculations are parameter free, they demonstrate a very good agreement with data.

The ratio of ψ' to J/ψ photoproduction yields has drawn attention recently since previous calculations grossly underestimate the experimental values. It is demonstrated in Sec. III C that the Melosh spin transformation, which has been overlooked previously and accompanies the Lorentz boost, may be the reason. It has a dramatic impact on the ψ' photoproduction increasing its yield by a factor of 2–3, in a good agreement with the data.

After we will have demonstrated that the approach under discussion quantitatively explains the photoproduction data, we calculate in Sec. IV the total charmonium-nucleon cross sections for J/ψ, ψ', and χ's. We predict quite a steep energy dependence for these cross sections slightly varying for different charmonia. Although the cross sections correlate with the mean charmonium size, this dependence is slower than $\propto\langle r_T^2\rangle$, and this fact finds a simple explanation. In Sec. V we compare our estimates for charmonium-nucleon cross sections with the effective absorption cross section of charmonium which can be extracted from data on nuclear attenuation of J/ψ and ψ'. Agreement is rather good.

Our results are summarized in Sec. VI where we also discuss the physics of energy dependence of the cross sections and the status of our approach. Special attention is given to nuclear attenuation of charmonia which is affected by formation and coherence time phenomena in an important way.

II. LIGHT-CONE DIPOLE FORMALISM FOR VIRTUAL PHOTOPRODUCTION OF CHARMONIA OFF NUCLEONS

The light-cone variable describing longitudinal motion which is invariant to Lorentz boosts is the fraction $\alpha=p_c^+/p_{\gamma^*}^+$ of the photon light-cone momentum $p_{\gamma^*}^+=E_{\gamma^*}+p_{\gamma^*}$ carried by the quark or antiquark. In the nonrelativistic approximation (assuming no relative motion of c and $\bar{c}$) $\alpha=1/2$ (e.g., [3]); otherwise one should integrate over α [see Eq. (1)]. For transversely (T) and longitudinally (L) polarized photons the perturbative photon-quark distribution function in Eq. (1) reads [4,5]

$$\Phi_{T,L}^{(\mu,\bar{\mu})}(\alpha,\vec{r}_T,Q^2)=\frac{\sqrt{N_c\alpha_{em}}}{2\pi}Z_c\chi_c^{\mu\dagger}\hat{O}_{T,L}\tilde{\chi}_{\bar{c}}^{\bar{\mu}}K_0(\epsilon r_T), \tag{3}$$

where

$$\tilde{\chi}_{\bar{c}}=i\sigma_y\chi_{\bar{c}}^*; \tag{4}$$

χ and $\bar{\chi}$ are the spinors of the c quark and antiquark, respectively; $Z_c=2/3$. $K_0(\epsilon r_T)$ is the modified Bessel function with

$$\epsilon^2=\alpha(1-\alpha)Q^2+m_c^2. \tag{5}$$

The operators $\hat{O}_{T,L}$ have the form

$$\hat{O}_T=m_c\vec{\sigma}\cdot\vec{e}_\gamma+i(1-2\alpha)(\vec{\sigma}\cdot\vec{n})(\vec{e}_\gamma\cdot\vec{\nabla}_{r_T})+(\vec{n}\times\vec{e}_\gamma)\cdot\vec{\nabla}_{r_T}, \tag{6}$$

$$\hat{O}_L=2Q\alpha(1-\alpha)\vec{\sigma}\cdot\vec{n}, \tag{7}$$

where $\vec{n}=\vec{p}/p$ is a unit vector parallel to the photon momentum and $\vec{e}$ is the polarization vector of the photon. Effects of the nonperturbative interaction within the $q\bar{q}$ fluctuation are negligible for the heavy charmed quarks.

The color dipole cross section $\sigma_{q\bar{q}}(r_T,s)$ is poorly known from first principles. It is expected to vanish $\propto r_T^2$ at small $r_T\to 0$ due to color screening [6] and to level off at large separations due to a finite range of gluon propagation. We employ phenomenological approaches described in Sec. II A.

The charmonium wave function is well defined in the rest frame where one can rely on the Schrödinger equation. We present solutions for four potentials proposed in the literature (Sec. II B). As soon as the rest frame wave function is known, one may be tempted to apply the Lorentz transformation to the $c\bar{c}$ pair as it would be a classical system and boost it to the infinite-momentum frame. However, quantum effects are important and in the infinite-momentum frame a series of different Fock states emerges from the Lorentz boost. (Compare with a Lorentz boost of a positronium: Weizsäker-Williams photons appear.) Therefore the lowest $|c\bar{c}\rangle$ component in the infinite-momentum frame does not represent the $|c\bar{c}\rangle$ in the rest frame. We rely on the widely used procedure for the generation of the light-cone wave functions of charmonia and describe it in Sec. II C.

A. Phenomenological dipole cross section

The dipole formalism for hadronic interactions introduced in [6] expands the hadronic cross section over the eigenstates of the interaction which in QCD are the dipoles with a definite transverse separation [see Eq. (1)]. Correspondingly, the values of the dipole cross section $\sigma_{q\bar{q}}(r_T)$ for different r_T are the eigenvalues of the elastic amplitude operator. This cross section is flavor invariant, due to the universality of the QCD coupling, and vanishes like $\sigma_{q\bar{q}}(r_T)\propto r_T^2$ for $r_T\to 0$. The latter property is sometimes referred to as color transparency.

The total cross sections for all hadrons and (virtual) photons are known to rise with energy. Apparently, the energy dependence cannot originate from the hadronic wave functions in Eqs. (1), (2), but only from the dipole cross section. In the approximation of two-gluon exchange used in [6] the dipole cross section is constant, the energy dependence originates from higher-order corrections related to gluon radiation. On the other hand, one can stay with two-gluon exchange, but involve higher Fock states which contain gluons in addition to the $q\bar{q}$. Both approaches correspond to the same set of Feynman graphs. We prefer to introduce energy dependence into $\sigma_{q\bar{q}}(r_T,s)$ and not include higher Fock states in the wave functions.

For the small size dipoles essential for deep inelastic scattering (DIS) one may apply perturbative QCD and the energy dependence comes as an effect of of gluon radiation treated in the leading-log$(1/x)$ approximation [7,8]. In the opposite limit of large separations typical for light hadrons one can also calculate the effects of gluon bremsstrahlung making use of smallness of the quark-gluon correlation radius [9].

However, the intermediate case we are interested in is the most complicated one as usual. No reliable way to sum up higher-order corrections is known so far. Therefore we use a phenomenological form which interpolates between the two limiting cases of small and large separations. Few parametrizations are available in the literature; we choose two of them which are simple, but quite successful in describing data and denote them by the initials of the authors as ‘‘GBW’’ [10] and ‘‘KST’’ [11].

We have

$$\text{‘‘GBW’’:}\quad \sigma_{q\bar{q}}(r_T,x)=23.03[1-e^{-r_T^2/r_0^2(x)}]\ \text{mb},$$

$$r_0(x)=0.4\left(\frac{x}{x_0}\right)^{0.144}\ \text{fm}, \tag{8}$$

where $x_0=3.04\times 10^{-4}$. The proton structure function calculated with this parametrization fits very well all available data at small x and for a wide range of Q^2 [10]. However, it obviously fails to describe the hadronic total cross sections, since it never exceeds the value 23.03 mb. The x dependence guarantees Bjorken scaling for DIS at high Q^2; however, the Bjorken x is not a well-defined quantity in the soft limit. Instead we use the prescription of [12], $x=(M_\psi^2+Q^2)/s$, where M_ψ is the charmonium mass.

This problem as well as the difficulty with the definition of x has been fixed in [11]. The dipole cross section is treated as a function of the c.m. energy $\sqrt{s}$, rather than x, since $\sqrt{s}$ is more appropriate for hadronic processes. A similarly simple form for the dipole cross section is used:

$$\text{‘‘KST’’:}\quad \sigma_{q\bar{q}}(r_T,s)=\sigma_0(s)[1-e^{-r_T^2/r_0^2(s)}]. \tag{9}$$

The values and energy dependence of hadronic cross sections is guaranteed by the choice of

$$\sigma_0(s)=23.6\left(\frac{s}{s_0}\right)^{0.08}\left(1+\frac{3}{8}\frac{r_0^2(s)}{\langle r_{ch}^2\rangle}\right)\ \text{mb}, \tag{10}$$

$$r_0(s)=0.88\left(\frac{s}{s_0}\right)^{-0.14}\ \text{fm}. \tag{11}$$

The energy-dependent radius $r_0(s)$ is fitted to data for the proton structure function $F_2^p(x,Q^2)$, $s_0=1000\ \text{GeV}^2$ and the mean square of the pion charge radius $\langle r_{ch}^2\rangle=0.44\ \text{fm}^2$. The improvement at large separations leads to a somewhat worse description of the proton structure function at large Q^2. Apparently, the cross section dependent on energy, rather than x, cannot provide Bjorken scaling. Indeed, parametrization (9) is successful only up to $Q^2\approx 10\ \text{GeV}^2$.

In fact, the cases we are interested in, charmonium production and interaction, are just in between the regions where either of these parametrizations is successful. Therefore, we suppose that the difference between predictions using Eqs. (8) and (9) is a measure of the theoretical uncertainty which fortunately turns out to be rather small.

We demontrate in Fig. 2 a few examples of r_T^2 dependence of the dipole cross section at different energies for both parametrizations. The KST cross section reveals a nontrivial behavior; it rises with energy at $r_T<3\ \text{fm}^2$, but decreases at larger separations. This is, however, a temporary effect; $\sigma_0(s)$ reaches the minimum at $\sqrt{s}\approx 77\ \text{GeV}$ and then slowly rises at higher energies. Such a peculiar behavior is a consequence of our original intention to reproduce the energy dependence of the hadronic cross sections $\sigma_{tot}^{hp}\propto s^{0.08}$ keeping the form (9) of the cross section. Of course data are insensitive to the cross section at such large separations.

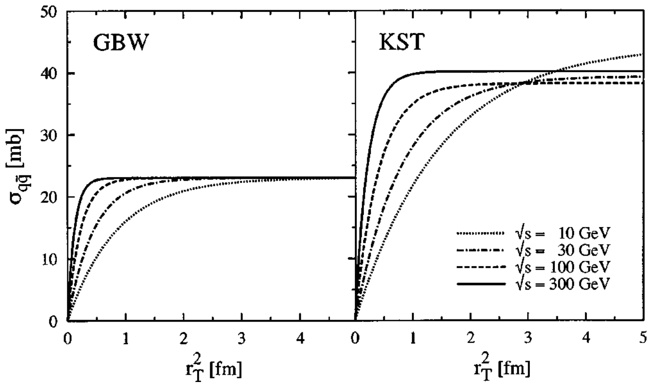

FIG. 2. The dipole cross section as function of r_T^2 at energies $\sqrt{s}=10$, 30, 100, and 300 GeV for GBW (left) and KST (right) parametrizations.

Both GBW and KST cross sections vanish $\propto r_T^2$ at small r_T; however, they considerably deviate from this simple behavior at large separations. Quite often, the simplest parametrization ($\propto r_T^2$) for the dipole cross section is used. For the coefficient in front of r_T^2 we employ the expression obtained by the first term of the Taylor expansion of Eq. (9):

$$\text{``}r_T^2\text{'':}\quad \sigma_{q\bar{q}}(r_T,s)=\frac{\sigma_0(s)}{r_0^2(s)}r_T^2. \tag{12}$$

B. Charmonium wave functions

The spatial part of the $c\bar{c}$ pair wave function satisfying the Schrödinger equation

$$\left(-\frac{\Delta}{m_c}+V(r)\right)\Psi_{nlm}(\vec{r})=E_{nl}\Psi_{nlm}(\vec{r}) \tag{13}$$

is represented in the form

$$\Psi(\vec{r})=\Psi_{nl}(r)\cdot Y_{lm}(\theta,\varphi), \tag{14}$$

where $\vec{r}$ is three-dimensional $c\bar{c}$ separation, and $\Psi_{nl}(r)$ and $Y_{lm}(\theta,\varphi)$ are the radial and orbital parts of the wave function. The equation for radial $\Psi(r)$ is solved with the help of the program in [13]. The following four potentials $V(r)$ have been used (see Fig. 3).

(i) ''COR'': Cornell potential [14],

$$V(r)=-\frac{k}{r}+\frac{r}{a^2}, \tag{15}$$

with $k=0.52$, $a=2.34\ \text{GeV}^{-1}$, and $m_c=1.84\ \text{GeV}$.

(ii) ''BT'': potential suggested by Buchmüller and Tye [15] with $m_c=1.48\ \text{GeV}$. It has a similar structure as the Cornell potential: linear string potential at large separations and Coulomb shape at short distances with some refinements, however.

(iii) ''LOG'': logarithmic potential [16]

$$V(r)=-0.6635\ \text{GeV}+(0.733\ \text{GeV})\log(r\times 1\ \text{GeV}), \tag{16}$$

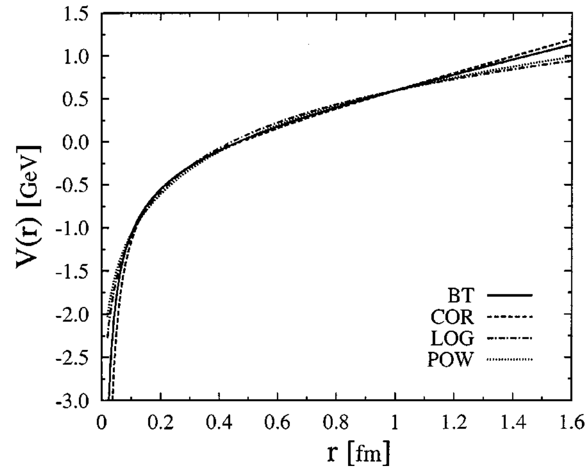

FIG. 3. Shapes of the potentials $V(r)$ for the four parametrizations employed in this paper. The curves for COR, LOG, and POW are normalized at $r=1$ fm to the value of the BT potential.

with $m_c=1.5\ \text{GeV}$.

(iv) ''POW'': power-law potential [17]

$$V(r)=-8.064\ \text{GeV}+(6.898\ \text{GeV})(r\times 1\ \text{GeV})^{0.1}, \tag{17}$$

with $m_c=1.8\ \text{GeV}$.

The shapes of the four potentials are displayed in Fig. 3 and differ from each other only at large r ($\geqslant 1$ fm) and very small r ($\leqslant 0.05$ fm) separations. Note, however, that COR and POW use $m_c\approx 1.8\ \text{GeV}$, while BT and LOG use $m_c\approx 1.5\ \text{GeV}$ for the mass of the charmed quark. This difference will have significant consequences.

The results of calculations for the radial part $\Psi_{nl}(r)$ of the $1S$ and $2S$ states are depicted in Fig. 4. For the ground state all the potentials provide a very similar behavior for $r>0.3$ fm, while for small r the predictions are different by up to 30%. The peculiar property of the $2S$-state wave function is the node at $r\approx 0.4$ fm which causes strong cancellations in the matrix elements, Eq. (1), and, as a result, a suppression of photoproduction of ψ' relative to J/ψ [3,18].

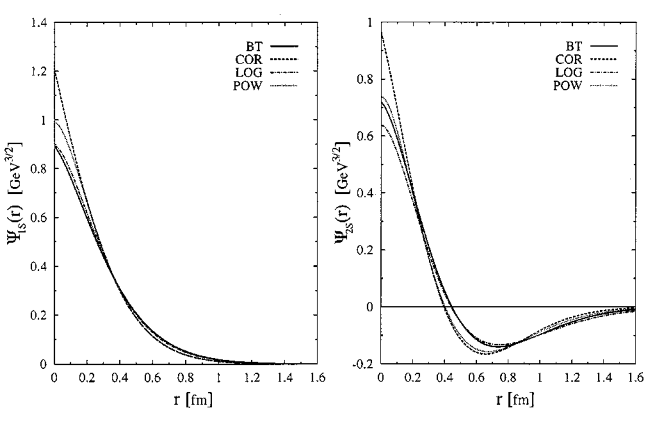

FIG. 4. The radial part of the wave function $\Psi_{nl}(r)$ for the $1S$ and $2S$ states calculated with four different potentials (see text).

C. Light-cone wave functions for the bound states

As has been mentioned, the lowest Fock component $|c\bar{c}\rangle$ in the infinite-momentum frame is not related by a simple Lorentz boost to the wave function of charmonium in the rest frame. This makes the problem of building the light-cone wave function for the lowest $|c\bar{c}\rangle$ component difficult; no unambiguous solution is yet known. There are only recipes in the literature; a simple one widely used [19] is the following. One applies a Fourier transformation from coordinate to momentum space to the known spatial part of the nonrelativistic wave function (14), $\Psi(\vec{r})\Rightarrow\Psi(\vec{p})$, which can be written as a function of the effective mass of the $c\bar{c}$, $M^2=4(p^2+m_c^2)$, expressed in terms of light-cone variables:

$$M^2(\alpha,p_T)=\frac{p_T^2+m_c^2}{\alpha(1-\alpha)}. \tag{18}$$

In order to change integration variable p_L to the light-cone variable α one relates them via M, namely, $p_L=(\alpha-1/2)M(p_T,\alpha)$. In this way the $c\bar{c}$ wave function acquires a kinematical factor

$$\Psi(\vec{p})\Rightarrow\sqrt{2}\frac{(p^2+m_c^2)^{3/4}}{(p_T^2+m_c^2)^{1/2}}\Psi(\alpha,\vec{p}_T)\equiv\Phi_\psi(\alpha,\vec{p}_T). \tag{19}$$

This procedure is used in [20] and the result is applied to the calculation of the amplitudes (1). The result is discouraging, since the ψ' to J/ψ ratio of the photoproduction cross sections is far too low in comparison with the data. However, an oversimplified dipole cross section $\sigma_{q\bar{q}}(r_T)\propto r_T^2$ has been used, and what is even more essential, the important ingredient of Lorentz transformations, the Melosh spin rotation, has been left out. The spin transformation has also been left out in a recent publication [21] which repeats the calculations of [20] with a more realistic dipole cross section which levels off at large separations. This leads to a suppression of the node effect (less cancellation) and enhancement of ψ' photoproduction. Nevertheless, the calculated ψ' to J/ψ ratio is smaller than the data by a factor of two.

The two-dimensional spinors χ_c and $\chi_{\bar{c}}$ describing c and $\bar{c}$, respectively, in the infinite-momentum frame are known to be related via the Melosh rotation [22,19] to the spinors $\bar{\chi}_c$ and $\bar{\chi}_{\bar{c}}$ in the rest frame:

$$\begin{aligned}\bar{\chi}_{\mathbf{c}}&=\hat{R}(\alpha,\vec{p}_T)\chi_c,\\ \bar{\chi}_{\bar{\mathbf{c}}}&=\hat{R}(1-\alpha,-\vec{p}_T)\chi_{\bar{c}},\end{aligned} \tag{20}$$

where the matrix $R(\alpha,\vec{p}_T)$ has the form

$$\hat{R}(\alpha,\vec{p}_T)=\frac{m_c+\alpha M-i[\vec{\sigma}\times\vec{n}]\vec{p}_T}{\sqrt{(m_c+\alpha M)^2+p_T^2}}. \tag{21}$$

Since the potentials we use in Sec. II B contain no spin-orbit term, the $c\bar{c}$ pair is in the S wave. In this case spatial and spin dependences in the wave function factorize and we arrive at the following light-cone wave function of the $c\bar{c}$ in the infinite-momentum frame:

$$\Phi_\psi^{(\mu,\bar{\mu})}(\alpha,\vec{p}_T)=U^{(\mu,\bar{\mu})}(\alpha,\vec{p}_T)\cdot\Phi_\psi(\alpha,\vec{p}_T), \tag{22}$$

where

$$U^{(\mu,\bar{\mu})}(\alpha,\vec{p}_T)=\chi_c^{\mu\dagger}\hat{R}^\dagger(\alpha,\vec{p}_T)\vec{\sigma}\cdot\vec{e}_\psi\sigma_y\hat{R}^*\times(1-\alpha,-\vec{p}_T)\sigma_y^{-1}\tilde{\chi}_c^{\bar{\mu}} \tag{23}$$

and $\tilde{\chi}_{\bar{c}}$ is defined in Eq. (4).

Note that the wave function (22) is different from the one used in [23–25] where it was assumed that the vertex $\psi\to c\bar{c}$ has the structure $\psi_\mu\bar{u}\gamma_\mu u$ like for the photon $\gamma^*\to c\bar{c}$. The rest frame wave function corresponding to such a vertex contains the S wave and D wave. The weight of the latter is dictated by the structure of the vertex and cannot be justified by any reasonable nonrelativistic potential model for the $c\bar{c}$ interaction.

Now we can determine the light-cone wave function in the mixed longitudinal-momentum–transverse-coordinate representation:

$$\Phi_\psi^{(\mu,\bar{\mu})}(\alpha,\vec{r}_T)=\frac{1}{2\pi}\int d^2\vec{p}_T e^{-i\vec{p}_T\vec{r}_T}\Phi_\psi^{(\mu,\bar{\mu})}(\alpha,\vec{p}_T). \tag{24}$$

The spatial component $\Phi_\psi(\alpha,\vec{r}_T)$ of Eq. (19) in the mixed representation (24) is plotted as a function of r_T and α in Fig. 5 for $J/\psi(1S)$ and $\psi'(2S)$ states. While the $1S$ wave function depends monotonically on r_T and smoothly vanishes at small α, the wave function of the $2S$ state demonstrates a nontrivial behavior: the node disappears for small α.

III. CALCULATIONS AND COMPARISON WITH DATA

A. Final expressions

Having the light-cone wave function of charmonium in momentum representation, Eq. (22), it is more convenient to switch to an integration over $\vec{p}_T$ in the matrix element Eq. (1):

$$\mathcal{M}_{T,L}(s,Q^2)=\int_0^1 d\alpha\int d^2\vec{p}_T\Phi_\psi^*(\alpha,\vec{p}_T)\Sigma_{T,L}(\alpha,\vec{p}_T,s,Q^2), \tag{25}$$

where

$$\Sigma_{T,L}(\alpha,\vec{p}_T,s,Q^2)=\frac{1}{2\pi}\sum_{\mu,\bar{\mu}}U^{(\mu,\bar{\mu})}(\alpha,\vec{p}_T)\times\int d^2\vec{r}_T e^{i\vec{p}_T\vec{r}_T}\sigma(r_T,s)\Phi_{T,L}^{(\mu,\bar{\mu})}(\alpha,\vec{r}_T,Q^2). \tag{26}$$

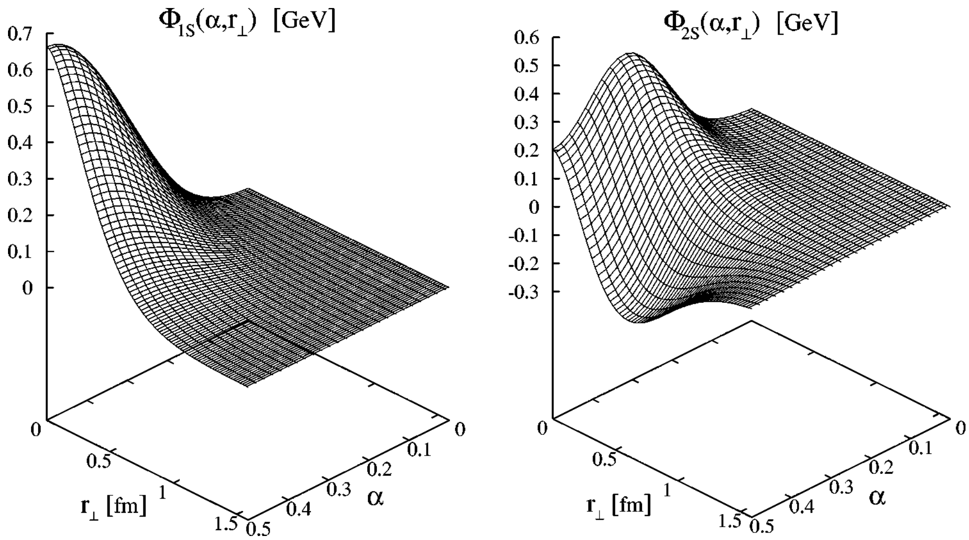

FIG. 5. Three-dimensional plot for the light-cone wave functions for $J/\psi(1S)$ and $\psi'(2S)$ in the mixed α-$\vec{r}_T$ representation for the BT potential [14].

If the dipole cross section depends on r_T like $\sigma_0(1-e^{-r_T^2/r_0^2})$ [see Eqs. (8) and (9)], then $\Sigma(\alpha,\vec{p}_T,s,Q^2)$, which includes the effects of spin rotation, can be expressed as follows:

$$\Sigma_T(\alpha,\vec{p}_T,s,Q^2)=\frac{1}{m_c}\left[m_T-\frac{2p_T^2\alpha(1-\alpha)}{m_T+m_L}\right]\tilde{\Sigma}_T(\alpha,\vec{p}_T,s,Q^2)-\frac{2p_T^2}{m_q m_T r_0^2}\left[1+\frac{m_T(1-2\alpha)}{m_T+m_L}\right]\times\frac{\partial\tilde{\Sigma}_t(\alpha,\vec{p}_T,s,Q^2)}{\partial p_T^2}, \tag{27}$$

$$\Sigma_L(\alpha,\vec{p}_T,s,Q^2)=\frac{m_q^2+m_T m_L}{m_c(m_T+m_L)}\tilde{\Sigma}_L(\alpha,\vec{p}_T,s,Q^2), \tag{28}$$

where $m_T^2=m_c^2+p_T^2$, $m_L^2=4m_c^2\alpha(1-\alpha)$ and

$$\tilde{\Sigma}_{T,L}(\alpha,\vec{p}_T,s,Q^2)=\frac{\sigma_0(s)}{2\pi}\int d^2r_T e^{i\vec{p}_T\vec{r}_T}\Phi_{T,L}(\alpha,\vec{r}_T,Q^2)\times[1-e^{-r_T^2/r_0^2(s)}], \tag{29}$$

$$\tilde{\Sigma}_t(\alpha,\vec{p}_T,s,Q^2)=\frac{\sigma_0(s)}{2\pi}\int d^2r_T e^{i\vec{p}_T\vec{r}_T}\Phi_T(\alpha,\vec{r}_T,Q^2)\times e^{-r_T^2/r_0^2(s)}, \tag{30}$$

$$\Phi_T(\alpha,r_T,Q^2)=\frac{1}{\pi}\sqrt{\frac{2\alpha_{em}}{3}}m_q K_0(\epsilon r_T), \tag{31}$$

$$\Phi_L(\alpha,r_T,Q^2)=\frac{2}{\pi}\sqrt{\frac{\alpha_{em}}{3}}Q\alpha(1-\alpha)K_0(\epsilon r_T). \tag{32}$$

The photoproduction cross section is given by

$$\sigma_{\gamma^*p\to\psi p}(s,Q^2)=\frac{|\tilde{\mathcal{M}}_T(s,Q^2)|^2+\varepsilon|\tilde{\mathcal{M}}_L(s,Q^2)|^2}{16\pi B}, \tag{33}$$

where ε is the photon polarization (for H1 data $\langle\varepsilon\rangle=0.99$); B is the slope parameter in reaction $\gamma^*p\to\psi p$. We use the experimental value [26] $B=4.73\ \mathrm{GeV}^{-2}$. $\tilde{\mathcal{M}}_{T,L}$ includes also the correction for the real part of the amplitude:

$$\tilde{\mathcal{M}}_{T,L}(s,Q^2)=\mathcal{M}_{T,L}(s,Q^2)\left(1-i\frac{\pi}{2}\frac{\partial\ln\mathcal{M}_{T,L}(s,Q^2)}{\partial\ln s}\right), \tag{34}$$

where we apply the well-known derivative analyticity relation between the real and imaginary parts of the forward elastic amplitude [27]. The correction from the real part is not small since the cross section of charmonium photoproduction is a rather steep function of energy (see below).

B. s and Q^2 dependence of $\sigma(\gamma^*p\to J/\psi p)$

Now we are in a position to calculate the cross section of charmonium photoproduction using Eq. (33). The results for J/ψ are compared with the data in Fig. 6. Calculations are performed with GBW and KST parametrizations for the dipole cross section and for wave functions of the J/ψ calculated from BT, LOG, COR, and POW potentials. One observes the following.

(i) There are no major differences for the results using the GBW and KST parametrizations.

(ii) The use of different potentials to generate the wave functions of the J/ψ leads to two distinctly different behaviors. The potentials labeled BT and LOG (see Sec. II B) describe the data very well, while the potentials COR and LOG underestimate them by a factor of 2. The different behavior has been traced to the following origin: BT and LOG use $m_c\approx1.5$ GeV, but COR and POW $m_c\approx1.8$ GeV. While the bound state wave functions of J/ψ are little affected by this difference (see Fig. 4), the photon wave function Eq. (3)

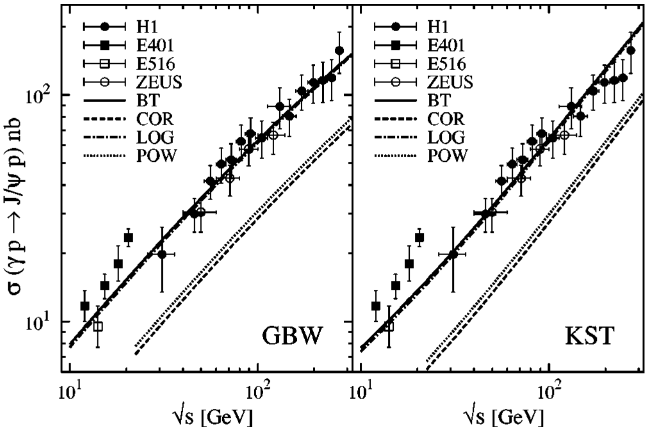

FIG. 6. Integrated cross section for elastic photoproduction $\gamma p \to J/\psi p$ with real photons ($Q^2=0$) as a function of the energy calculated with GBW and KST dipole cross sections and for four potentials to generate J/ψ wave functions. Experimental data points from the H1 [26], E401 [28], E516 [29], and ZEUS [30] experiments.

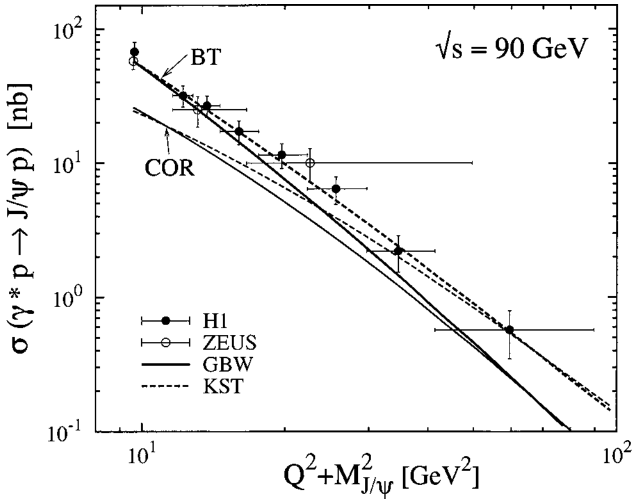

FIG. 7. Integrated cross section for elastic photoproduction as a function of the photon virtuality $Q^2+M_{J/\psi}$ at energy $\sqrt{s}=90$ GeV. Solid and dashed curves are calculated with GBW and KST dipole cross sections, while thick and thin curves correspond to BT and COR potentials, respectively. Results obtained with LOG and POW potentials are very close to those curves (LOG similar to BT and POW to COR; see also Fig. 6). Experimental data points from the H1 [37] and ZEUS [46] experiments.

depends sensitively on m_c via the argument Eq. (5) of the K_0 function.

We compare our calculations also with data for the Q^2 dependence of the cross section. The data are plotted in Fig. 7 at the c.m. energy $\sqrt{s}=90$ GeV as a function of $Q^2+M^2_{J/\psi}$, since in this form both the data and calculations display an approximate power law dependence.

Such a dependence on $Q^2+M^2_{J/\psi}$ is suggested by the variable ϵ^2 in Eq. (5), which for $\alpha=1/2$ takes the value $Q^2+(2m_c)^2$. It may be considered as an indication that $\alpha=1/2$ is a reasonable approximation for the nonrelativistic charmonium wave function.

Our results are depicted for BT and COR potentials and using GBW and KST cross sections. Agreement with the calculations based on BT potential is again quite good, while the COR potential grossly underestimates the data at small Q^2. Although the GBW and KST dipole cross sections lead to nearly the same cross sections for real photoproduction, their predictions at high Q^2 are different by a factor of 2–3. Supposedly the GBW parametrization should be more trustworthy at $Q^2 \gg M^2_{\psi}$.

C. Importance of spin effects for the ψ' to J/ψ ratio

It turns out that the effects of spin rotation have a gross impact on the cross section of elastic photoproduction $\gamma p \to J/\psi(\psi)p$. To demonstrate these effects we present the results of our calculations at $\sqrt{s}=90$ GeV in Table I.

The upper half of the table shows the photoproduction cross sections for J/ψ for different parametrizations of the dipole cross section (GBW, KST, "r_T^2") and potentials (BT, COR, LOG, POW). The numbers in parentheses show what the cross section would be if the spin rotation effects were neglected. We see that these effects add 30–40 % to the J/ψ photoproduction cross section.

The spin rotation effects turn out to have a much more dramatic impact on ψ', increasing the photoproduction cross section by a factor of 2–3. This is visible in the lower half of the table which shows the ratio $R=\sigma(\psi')/\sigma(J/\psi)$ of the photoproduction cross sections, where the number in parentheses correspond to no spin rotation effects included. This

TABLE I. The photoproduction $\gamma p \to J/\psi p$ cross section $\sigma(J/\psi)$ in nb and the ratio $R=\sigma(\psi')/\sigma(J/\psi)$ for the four different types of potentials (BT, LOG, COR, POW) and the three parametrizations (GBW, KST, r_T^2) for the dipole cross section $\sigma(r_T,s)$ at $\sqrt{s}=90$ GeV. The values in parentheses correspond to the case when the spin rotation is neglected.

		BT	LOG	COR	POW
σ	GBW	52.01 (37.77)	50.78 (36.63)	23.13 (17.07)	24.94 (18.64)
	KST	49.96 (35.87)	48.49 (34.57)	21.05 (15.42)	22.83 (16.92)
	r_T^2	66.67 (47.00)	64.07 (44.86)	25.81 (18.71)	28.23 (20.66)
R	GBW	0.147 (0.075)	0.117 (0.060)	0.168 (0.099)	0.144 (0.085)
	KST	0.147 (0.068)	0.118 (0.054)	0.178 (0.099)	0.152 (0.084)
	r_T^2	0.101 (0.034)	0.081 (0.027)	0.144 (0.070)	0.121 (0.058)

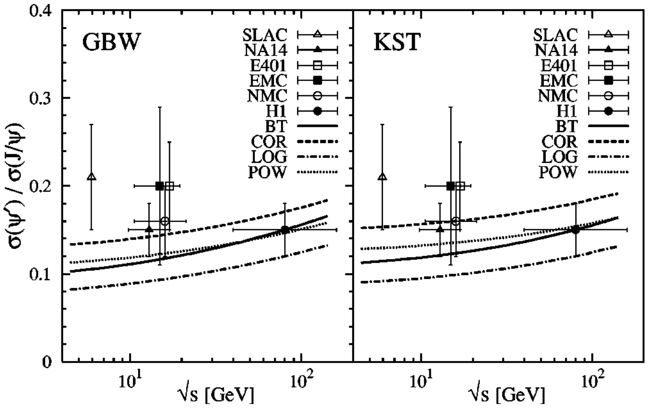

FIG. 8. The ratio of ψ' to J/ψ photoproduction cross sections as a function of c.m. energy calculated for all four potentials with with GBW and KST parametrizations for the dipole cross section. Experimental data points are from the SLAC [31], NA14 [32], E401 [33], EMC [34], NMC [35], and H1 [36] experiments.

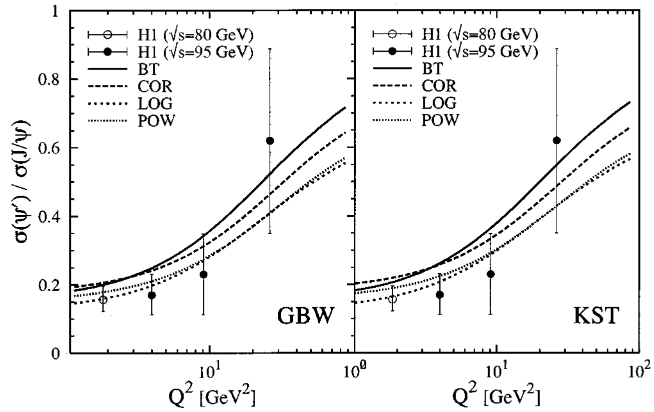

FIG. 9. The ratio of ψ' to J/ψ photoproduction cross sections as a function of the photon virtuality Q^2 at energy $\sqrt{s}=90$ GeV all four potentials with with GBW and KST parametrizations for the dipole cross section. Experimental data points from the H1 experiment [37].

spin effects explain the large values of the ratio R observed experimentally. Our results for R are about twice as large as evaluated in [21] and even more than in [20].

The ratio of ψ' to J/ψ photoproduction cross sections is depicted as function of c.m. energy in Fig. 8 and as a function of Q^2 in Fig. 9 for all four potentials and for the parametrizations of the dipole cross sections GBW and KST.

Our calculations agree with available data, but the error bars are too large to provide a more precise test for the theory. Remarkably, the ratio $R(s)$ rises with energy. This result is in variance with the naive expectation based on the larger size of the ψ' and on the usual rule: the smaller the size of the $q\bar{q}$ dipole, the steeper its energy dependence. There is, however, no contradiction, since this is another manifestation of the node in the wave function of ψ'. Indeed, as a function of energy mostly the short distance part of the dipole cross section $\sigma_{q\bar{q}}(r_T)$ rises. It enhances the positive contribution for distances shorter than the node position in the ψ' wave function. Therefore, with increasing energy the cancellation in the amplitude of ψ' production is reduced. This effect leads to a steeper energy dependence of ψ' production compared to J/ψ. The effect is stronger for GBW than KST parametrizations, since the GBW cross section does not rise with energy at all at large separations. Note that this situation is specific for photoproduction because the nodeless wave function of the photon is projected to the sign changing wave function of ψ'. This should not happen in the case of elastic $J/\psi(\psi')$-p scattering (see below).

Similarly of the node effect leads to a rising Q^2 dependence of the ψ' to J/ψ ratio in the photoproduction cross sections. Our calculations are compared with available data in Fig. 9 for the GBW and KST parametrizations, respectively.

IV. CHARMONIUM-NUCLEON TOTAL CROSS SECTIONS

After the light-cone formalism has been checked with the data for virtual photoproduction we are in position to provide reliable predictions for charmonium-nucleon total cross sections. The corresponding expressions are given by Eq. (2) (compare with [6]). For the GBW and KST dipole cross sections, which have the form $\sigma_0(1-e^{-r_T^2/r_0^2})$ [see Eqs. (8) and (9)], a summation over spin indexes in Eq. (2) gives, for the S states,

$$\mathcal{M}_{\psi p}(s)=\sigma_0\cdot\Bigg[1-\pi r_0^2\int_0^1 d\alpha\int_0^\infty dp_T \times\int_0^\infty dq_T U(\alpha,p_T)U(\alpha,q_T)V(\alpha,p_T,q_T)\Bigg], \tag{35}$$

where

$$U(\alpha,p_T)=p_T\Phi_\psi(\alpha,p_T)e^{-r_0^2p_T^2/4}\{[M_1^2(p_T)+p_T^2]\times[M_2^2(p_T)+p_T^2]\}^{-1/2}, \tag{36}$$

$$V(\alpha,p_T,q_T)=M_1(p_T)M_1(q_T)M_2(p_T)M_2(q_T)I_0(v)+[M_1(p_T)M_1(q_T)+M_1(p_T)M_2(q_T)]p_Tq_TI_1(v)+p_T^2q_T^2I_2(v), \tag{37}$$

$$M_1(p_T)=m_c+m_T\sqrt{\frac{\alpha}{1-\alpha}}, \tag{38}$$

$$M_2(p_T)=m_c+m_T\sqrt{\frac{1-\alpha}{\alpha}}, \tag{39}$$

$$v=\frac{1}{2}r_0^2p_Tq_T. \tag{40}$$

Here $m_T^2=m_c^2+p_T^2$; $\Phi_\psi(\alpha,p_T)$ is defined in Eq. (19); $I_{0,1,2}(v)$ are Bessel functions of imaginary argument.

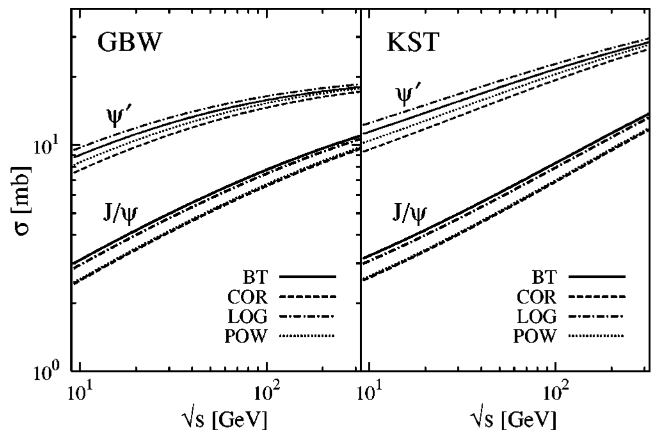

FIG. 10. Total $J/\psi p$ (thick curves) and $\psi' p$ (thin curves) cross sections with the GBW and KST parametrizations for the dipole cross section.

The calculated J/ψ- and ψ'-nucleon total cross sections are plotted in Fig. 10 for the GBW and KST forms of the dipole cross sections and all four types of charmonium potentials.

The corresponding results for χ states are depicted in Fig. 11.

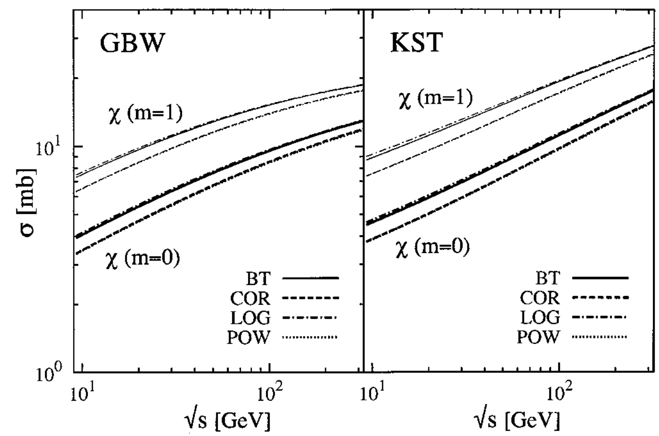

FIG. 11. Total χp ($m=0$, thick curves; $m=1$, thin curves) cross sections with the KST and GBW parametrizations for the dipole cross section.

Here m is the projection of the orbital momentum which can be 0 or 1, since this is a P-wave state. From these cross sections with definite m, which we denote σ_m^χ, one can construct the total cross sections for the χ_c states with different spins and helicities λ

$$
\begin{aligned}
\chi_{c0}(\lambda=0):&\quad \sigma=\frac{1}{3}(2\sigma_1^\chi+\sigma_0^\chi);\\
\chi_{c1}(\lambda=0):&\quad \sigma=\sigma_1^\chi;\\
\chi_{c1}(\lambda=\pm 1):&\quad \sigma=\frac{1}{2}(\sigma_1^\chi+\sigma_0^\chi);\\
\chi_{c2}(\lambda=0):&\quad \sigma=\frac{1}{3}(\sigma_1^\chi+2\sigma_0^\chi);\\
\chi_{c2}(\lambda=\pm 1):&\quad \sigma=\frac{1}{2}(\sigma_1^\chi+\sigma_0^\chi);\\
\chi_{c2}(\lambda=\pm 2):&\quad \sigma=\sigma_1^\chi.
\end{aligned}
\tag{41}
$$

Using these relations one can easily derive the cross sections averaged over helicities which are equal for all three states $\chi_{c0,1,2}$.

The strong dependence of the cross sections for P-wave charmonium states on the projection $m=0,1$ of the orbital momentum has been found previously in [38]. However, the predicted cross sections at $\sqrt{s}=10$ GeV for $\chi_c(m=0)$, $\chi_c(m=1)$, and ψ' are about twice as large as ours. We believe that the disagreement originates from the too rough nonperturbative dipole cross section[1] used in [38] which was not well adjusted to the data. Even the pion-nucleon cross section calculated with Eq. (1) in [38] overestimates the experimental value by a factor of 1.5.

Although all four potentials are presented, comparison with photoproduction data in Figs. 6 and 7 show that two of them, BT and LOG potentials, are more trustable at least for J/ψ. These two potentials again give very close predictions for J/ψ-p total cross sections but the deviation from the predictions with the two other potentials, COR and POW, is much smaller than in the case of photoproduction.

Note that the cross sections calculated with the GBW parametrization demonstrate a tendency to level off at very high energy, especially for ψ', as compared to the KST predictions. The reason is obvious: the GBW cross sections approach the universal limit $\sigma_{max}=\sigma_0=23.03$ mb. This cannot be true, and the KST parametrization is more reliable than GBW at high energies where the gluon cloud surrounding the $\bar{c}c$ pair becomes nearly as big as light hadrons.

According to Figs. 10 and 11 for the KST parametrization the total cross sections of charmonia are nearly straight lines as function of $\sqrt{s}$ in a double logarithmic representation, though with significantly different slopes for the different states. Therefore a parametrization in the form

$$\sigma^{\psi p}(s)=\sigma_0^\psi\left(\frac{s}{s_0}\right)^\Delta \tag{42}$$

seems appropriate, at least within a restricted energy interval. We use the data shown in Figs. 10 and 11 for the KST parametrization of $\sigma_{q\bar{q}}$ and for the BT and LOG potentials and fit the them by the form (42) with $s_0=1000$ GeV. The two values from the BT and LOG potentials have been averaged and their half difference gives the error estimation.

[1]We are thankful to Lars Gerland who provided us with the expression for the dipole cross section used in [38].

TABLE II. Averaged sizes $\langle r_T^2\rangle$ for charmonia bound states together with σ_0 and Δ in the parametrization (42) for the J/ψ-, ψ'-, and χ-proton cross sections. Estimation of the errors is given in the text.

	$\langle r_T^2\rangle$ [fm^2]	σ_0^ψ [mb]	Δ
J/ψ	0.117 ± 0.003	5.59 ± 0.13	0.212 ± 0.001
$\chi(m=0)$	0.181 ± 0.004	7.17 ± 0.07	0.195 ± 0.001
$\chi(m=1)$	0.362 ± 0.007	13.17 ± 0.16	0.164 ± 0.002
ψ'	0.517 ± 0.034	16.63 ± 0.59	0.139 ± 0.005

Table II shows values for σ_0^ψ and Δ averaged over the energy interval 10 GeV$<\sqrt{s}<$300 GeV and the bound state sizes $\langle r_T^2\rangle$.

As expected σ_0^ψ rises monotonically with the size of the charmonium state, and the cross section for $\psi' N$ is about 3 times larger than that for J/ψ. This deviates from the r_T^2 scaling, since the mean value $\langle r_T^2\rangle$ is 4 times larger for ψ' than for J/ψ. The exponent Δ which governs the energy dependence decreases monotonically with the size of the charmonium state, demonstrating the usual correlation between the dipole size and the steepness of energy dependence. The values of Δ are larger than in soft interactions of light hadrons (~0.08), but smaller than values reached in DIS at high Q^2.

Our results at $\sqrt{s}=10$ GeV [the mean energy of charmonia produced in the NA38/NA50 experiments at the Super Proton Synchrotron (SPS), CERN],

$$\sigma_{tot}^{J/\psi}(\sqrt{s}=10\ \text{GeV})=3.56\pm0.08\ \text{mb}, \tag{43}$$

$$\sigma_{tot}^{\psi'}(\sqrt{s}=10\ \text{GeV})=12.19\pm0.61\ \text{mb}, \tag{44}$$

agree well with the cross sections extracted in [2] from photoproduction data employing the two-channel approximation, 2.8 ± 0.12 mb$<\sigma_{tot}^{J/\psi}(\sqrt{s}=10\ \text{GeV})<4.1\pm0.15$ mb and $\sigma_{tot}^{\psi'}/\sigma_{tot}^{J/\psi}\approx3.75$ (having poorly controlled accuracy), which shows that the two-channel approach is a reasonable tool to analyze photoproduction data.

The cross section, Eq. (42), with the parameters in Table II agrees well with $\sigma_{tot}^{J/\psi}(\sqrt{s}=20\ \text{GeV})=4.4\pm0.6$ mb obtained in the model of the stochastic vacuum [39].

It is worth noting that the results for charmonium-nucleon total cross sections are amazingly similar to what one could get without any spin rotation,

$$\sigma_{tot}^{\psi N}(s)\approx\int_0^1 d\alpha\int d^2\vec{r}_T|\Phi_\psi(\alpha,\vec{r}_T)|^2\sigma_{q\bar{q}}(r_T,s), \tag{45}$$

where $\Phi_\psi(\alpha,\vec{r}_T)$ is related by Fourier transformation to Eq. (19), or even performing a simplest integration using the nonrelativistic wave functions (13) in the rest frame of the charmonium:

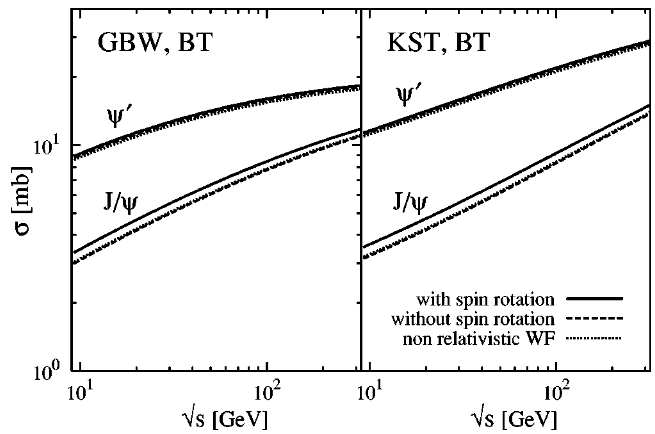

FIG. 12. Comparison of the results for $\sigma_{tot}^{\psi N}(s)$ obtained with the exact expression (2) (solid curves) and with the approximations (45) (dashed lines) and (46) (dotted lines).

$$\sigma_{tot}^{\psi N}(s)\approx\int d^3r|\Psi(\vec{r})|^2\sigma_{q\bar{q}}(r_T,s). \tag{46}$$

The comparison presented in Fig. 12 for the BT potential shows that Eqs. (45), (46) are only about 10% below the exact calculation for J/ψ, while there is practically no difference between the exact and approximate calculations for ψ'.

V. NUCLEAR SUPPRESSION OF CHARMONIUM PRODUCTION

Production of charmonia off nuclei seem to be a natural source of information about charmonium-nucleon cross section since nuclear absorption leads to suppression of the production rate measured experimentally. However, one should be cautious in applying our results to a calculation of the nuclear attenuation of charmonium. In exclusive photoproduction of charmonia the uncertainty principle does not allow one to resolve between J/ψ and ψ' unless the formation time $t_f=2E_\psi/(M_{\psi'}^2-M_{J/\psi}^2)$ [3,40] is shorter than the mean internucleon separation in nuclei. Only one experiment [41] at ~20 GeV satisfies this condition. Analyzed with an optical model it leads to $\sigma_{in}^{J/\psi N}=3.5\pm0.8$ mb in good agreement with our calculations. The nuclear photoproduction data [42] taken at 120 GeV cannot be treated in the same way since the formation time $l_f\approx10$ fm exceeds the nuclear size. In addition, the coherence length $l_c=2E_\psi/(M_{J/\psi}^2+Q^2)$ [3,43] is also long, about 5 fm, substantially increasing the attenuation path for the produced $\bar{c}c$ pair.

In the case of hadroproduction of charmonia off nuclei, the interplay of the formation and coherence time effects are as important as in photoproduction. On top of that, the situation is complicated by decays of χ's and ψ' which substantially feed the yield of J/ψ. These heavier states, even if their absorption cross sections are known from our calculations, are also subject to the effects of formation and coherence lengths.

In the analysis [44] of data from the experiment E866 of $pA\to J/\psi X$ collisions at 800 GeV, proper attention has been given to coherence and formation time effects with the result

TABLE III. Values for the J/ψ-, ψ'-, χ-, and effective ''J/ψ''-proton cross sections at energy $\sqrt{s}=10$ GeV. Errors are given by averaging on BT and LOG potentials for the wave functions.

	w_i	σ [mb]
J/ψ	0.52 - 0.6	3.56 ± 0.08
$\chi(m=0)$	0	4.66 ± 0.06
$\chi(m=1)$	0.32 - 0.4	9.05 ± 0.16
ψ'	0.08	12.19 ± 0.61

(extrapolated to $\sqrt{s}=10$ GeV)

$$\sigma_{eff}^{``J/\psi''p}=5.0\pm0.4 \ \text{mb}, \tag{47}$$

$$\sigma_{tot}^{\psi' p}=10.5\pm3.6 \ \text{mb}. \tag{48}$$

The effective J/ψ-nucleon cross section which is fed by decays of heavier states can be estimated as follows:

$$\frac{1}{\sigma_{eff}}(1-e^{-\sigma_{eff}\langle T\rangle})=\sum_{i=1}^{4}\frac{w_i}{\sigma_{tot}^{\psi_i N}}(1-e^{-\sigma_{tot}^{\psi_i N}\langle T\rangle}), \tag{49}$$

where $\langle T\rangle\approx0.75\rho_A R_A$ is the mean thickness of a nucleus with radius R_A and the mean density $\rho_A\approx0.16$ fm^{-3}.

Equation (49) is relevant for J/ψ suppression in nuclear collisions (proton-nucleus and nucleus-nucleus). In this reaction the observed J/ψ arises from directly produced J/ψ's with probability $w_1<1$ and from the other states χ, ψ' via decay after the charmonia have left the interaction zone, where w_i is the probability that the state i contributes to the finally observed J/ψ. Values for w_i and $\sigma_{tot}^{\psi_i p}$ are given in Table III where $m=0,1$ is the projection of the orbital momentum of the $\bar{c}c$ pair on the direction of gluon-gluon collision in $\chi_{1,2}$ production (χ_0 has a tiny branching to J/ψ).

It turns out that χ_1 and χ_2 with $m=0$ cannot be produced or are strongly suppressed in gluon fusion due to the selection rules which forbid projections ±1 for the total angular momentum (e.g., see [45]); this is why we put $w_2=0$.

We calculate σ_{eff} for tungsten used in the analysis [44] and find, for $\sqrt{s}=10$ GeV,

$$\sigma_{eff}^{``J/\psi''p}=5.8\pm0.2 \ \text{mb}, \tag{50}$$

where the main uncertainty arises from the w_i. This number is in a good accord with Eq. (47), while the calculated value for $\sigma_{tot}^{\psi' p}$, Eq. (44), agrees well with Eq. (48).

The coherence effects are quite important even at the energy of the NA38/NA50 experiments ($E_\psi\approx50$ GeV) at CERN; this is why the effective absorption cross section for ψ' production suggested by the data is about a half of the value we predict. At the energies of the BNL Relativistic Heavy Ion Collider (RHIC) and CERN Large Hadron Collider (LHC) both the coherence and formation times substantially exceed the sizes of heavy nuclei, and shadowing becomes the dominant phenomenon.

VI. CONCLUSION AND DISCUSSIONS

In this paper we have proposed a simultaneous treatment of elastic photoproduction $\sigma_{\gamma^* p\to\psi p}(s,Q^2)$ of charmonia and total cross sections $\sigma_{tot}^{\psi p}(s)$. The ingredients are (i) the factorized light-cone expressions (1),(2) for the cross sections, (ii) the perturbative light-cone wave functions for the $c\bar{c}$ component of the γ^*, (iii) light-cone wave functions for the charmonia bound states, and (iv) a phenomenological dipole cross section $\sigma_{q\bar{q}}(r_T,s)$ for a $c\bar{c}$ interacting with a proton.

The dipole cross section rises with energy; the smaller the transverse $\bar{q}q$ separation, the steeper the growth. The source of the energy dependence is the expanding cloud of gluons surrounding the $\bar{q}q$ pair. The gluon bremsstrahlung is more intensive for small dipoles. The gluon cloud can be treated as a joint contribution of higher Fock states, $|\bar{q}qnG\rangle$; however, it can be also included in the energy dependence of $\sigma_{q\bar{q}}(r_T,s)$, as we do, and this is the full description. The addition of any higher Fock state would be double counting.

As a function of energy the initial size of the $\bar{q}q$ source is gradually ''forgotten'' after multistep radiation; the small cross sections grow steeper and eventually approach the larger ones at very high energies. All the cross sections are expected to reach a universal asymptotic behavior which saturates the Froissart bound.

The effective dipole cross section $\sigma_{q\bar{q}}(r_T,s)$ is parametrized in a form which satisfies the expectations $\sigma_{q\bar{q}}\propto r_T^2$ for $r_T\to0$ (color transparency), but levels off for $r_T\to\infty$. Two parametrizations for $\sigma_{q\bar{q}}(r_T,s)$, whose form and parameters have been fitted to describe $\sigma_{tot}^{\pi p}(s)$, and the structure function $F_2(x,Q^2)$ are used in our calculations.

While the description of the photon wave function is quite certain, the light-cone wave function of charmonia is rather ambiguous. We have followed the usual recipe in going from a nonrelativistic wave function calculated from a Schrödinger equation to a light-cone form. We have included the Melosh spin rotation which is often neglected and found that it is instrumental to obtain agreement, since no parameter is adjustable. In particular, it increases the ψ' photoproduction cross section by a factor of 2–3 and rises the ψ' to J/ψ ratio to the experimental value.

At the same time, the charmonium-nucleon total cross sections [J/ψ, ψ', $\chi(m=0)$ and $\chi(m=1)$] turn out to be rather insensitive to how the light-cone wave function is formed; even applying no Lorentz transformation one arrives at nearly the same results. This is why we believe that the predicted charmonium-nucleon cross sections are very stable against the ambiguities in the light-cone wave function of charmonia. A significant energy dependence is predicted which varies from state to state in accordance with our expectations.

We show our predictions for charmonium-nucleon cross sections in a restricted energy range 10 GeV$<\sqrt{s}$ <300 GeV, but this interval can be largely extended in both directions. Since the Okubo-Zweig Iizuka (OZI) rule suppresses the leading Reggeons, one can stay with gluonic exchanges rather far down to low energies, unless the charmed Reggeon exchanges become important [47].

ACKNOWLEDGMENTS

This work has been supported by a grant from the Gesellschaft für Schwerionenforschung Darmstadt (GSI), Grant No. HD HÜFT, and by Federal Ministry BMBF Grant No. 06 HD 954.

[1] T. Matsui and H. Satz, Phys. Lett. B **178**, 416 (1986).
[2] J. Hüfner and B. Z. Kopeliovich, Phys. Lett. B **426**, 154 (1998).
[3] B. Z. Kopeliovich and B. G. Zakharov, Phys. Rev. D **44**, 3466 (1991).
[4] J. B. Kogut and D. E. Soper, Phys. Rev. D **1**, 2901 (1970).
[5] J. M. Bjorken, J. B. Kogut, and D. E. Soper, Phys. Rev. D **3**, 1382 (1971).
[6] A. B. Zamolodchikov, B. Z. Kopeliovich, and L. I. Lapidus, Pis'ma Zh. Éksp. Teor. Fiz. **33**, 612 (1981) [JETP Lett. **33**, 595 (1981)].
[7] L. N. Lipatov, Zh. Éksp. Teor. Fiz. **90**, 1536 (1986) [Sov. Phys. JETP **63**, 904 (1986)].
[8] Yu. L. Dokshitzer, V. A. Khoze, A. H. Mueller, and S. I. Troyan, *Basics of Perturbative QCD* (Editions Frontieres, Paris, 1991).
[9] B. Z. Kopeliovich, I. K. Potashnikova, B. Povh, and E. Predazzi, Phys. Rev. Lett. **85**, 507 (2000).
[10] K. Golec-Biernat and M. Wüsthoff, Phys. Rev. D **59**, 014017 (1999); **60**, 114023 (1999).
[11] B. Kopeliovich, A. Schäfer, and A. Tarasov, Phys. Rev. D **62**, 054022 (2000).
[12] M. G. Ryskin, R. G. Roberts, A. D. Martin, and E. M. Levin, Z. Phys. C **76**, 231 (1997).
[13] W. Lucha and F. F. Schöberl, Int. J. Mod. Phys. C **10**, 607 (1999).
[14] E. Eichten, K. Gottfried, T. Konoshita, K. D. Lane, and T.-M. Yan, Phys. Rev. D **17**, 3090 (1978); **21**, 203 (1980).
[15] A. Buchmüller and S.-H. H. Tye, Phys. Rev. D **24**, 132 (1981).
[16] C. Quigg and J. L. Rosner, Phys. Lett. **71B**, 153 (1977).
[17] A. Martin, Phys. Lett. **93B**, 338 (1980).
[18] O. Benhar, B. Z. Kopeliovich, Ch. Mariotti, N. N. Nikolaev, and B. G. Zakharov, Phys. Rev. Lett. **69**, 1156 (1992).
[19] M. V. Terent'ev, Yad. Fiz. **24**, 53 (1976) [Sov. J. Nucl. Phys. **24**, 106 (1976)].
[20] P. Hoyer and S. Peigné, Phys. Rev. D **61**, 031501(R) (2000).
[21] K. Suzuki *et al.*, Phys. Rev. D **62**, 031501(R) (2000).
[22] H. J. Melosh, Phys. Rev. D **9**, 1095 (1974); W. Jaus, *ibid.* **41**, 3394 (1990).
[23] M. G. Ryskin, Z. Phys. C **37**, 89 (1993).
[24] S. J. Brodsky *et al.*, Phys. Rev. D **50**, 3134 (1994); L. L. Frankfurt, W. Koepf, and M. I. Strikman, *ibid.* **54**, 3194 (1996).
[25] J. Nemchik *et al.*, Z. Phys. C **75**, 71 (1997).
[26] H1 Collaboration, C. Adloff *et al.*, Phys. Lett. B **483**, 23 (2000).
[27] J. B. Bronzan, G. L. Kane, and U. P. Sukhatme, Phys. Lett. **49B**, 272 (1974).
[28] E401 Collaboration, M. Binkley *et al.*, Phys. Rev. Lett. **48**, 73 (1982).
[29] E516 Collaboration, B. H. Denby *et al.*, Phys. Rev. Lett. **52**, 795 (1984).
[30] ZEUS Collaboration, J. Breitweg *et al.*, Z. Phys. C **75**, 215 (1997).
[31] U. Camerini *et al.*, Phys. Rev. Lett. **35**, 483 (1975).
[32] NA14 Collaboration, R. Barate *et al.*, Z. Phys. C **33**, 505 (1987).
[33] E401 Collaboration, M. Binkley *et al.*, Phys. Rev. Lett. **50**, 302 (1983).
[34] EMC Collaboration, J. J. Aubert *et al.*, Nucl. Phys. **B213**, 1 (1983).
[35] NMC Collaboration, P. Amaudraz *et al.*, Nucl. Phys. **B371**, 553 (1992).
[36] H1 Collaboration, C. Adloff *et al.*, Phys. Lett. B **421**, 385 (1998).
[37] H1 Collaboration, C. Adloff *et al.*, Eur. Phys. J. C **10**, 373 (1999).
[38] L. Gerland, L. Frankfurt, M. Strikman, H. Stöcker, and W. Greiner, Phys. Rev. Lett. **81**, 762 (1998).
[39] H. G. Dosch, F. S. Navarra, M. Nielsen, and M. Rueter, Phys. Lett. B **466**, 363 (1999); H. G. Dosch, T. Gousset, G. Kulzinger, and H. J. Pirner, Phys. Rev. D **55**, 2602 (1997).
[40] J. Hüfner and B. Z. Kopeliovich, Phys. Rev. Lett. **76**, 192 (1996).
[41] R. L. Anderson *et al.*, Phys. Rev. Lett. **38**, 263 (1977).
[42] M. D. Sokoloff *et al.*, Phys. Rev. Lett. **57**, 3003 (1986).
[43] J. Hüfner, B. Z. Kopeliovich, and J. Nemchik, Phys. Lett. B **383**, 362 (1996).
[44] Y. B. He, J. Hüfner, and B. Z. Kopeliovich, Phys. Lett. B **477**, 93 (2000).
[45] M. Vanttinen *et al.*, Phys. Rev. D **51**, 3332 (1995).
[46] ZEUS Collaboration, J. Breitweg *et al.*, Eur. Phys. J. C **6**, 603 (1999).
[47] T. Barnes, E. S. Swanson, and C. Y. Wong, ''Charmonium + Light Hadron Cross Sections,'' nucl-th/0006012.